Front. Chem. China 2011, 6(3): 227–242
DOI 10.1007/s11458-011-0241-x

RESEARCH ARTICLE

Vibrational dynamics of Ni-glassy alloys

Aditya M. VORA (✉)

The well known model potential is used to investigate the vibrational properties of some Ni-based binary glassy alloys using three theoretical models. Different local field correction functions are employed to see the effect of exchange and correlation in the aforesaid properties and have been found successful.

Keywords pseudopotential, pair potential, phonon dispersion curves (PDC), Ni-based amorphous binary alloys, local field correction functions

1 Introduction

The mankind has been manufacturing glassy materials for several thousand years. Compared to that, the scientific study of amorphous materials has a much shorter history. And only recently, there has been an explosion of interest to these studies as more promising materials are produced in the amorphous form. The range of applications of metallic glasses is vast and extends from the common window glass to high capacity storage media for digital devices [1–23].

The $Ni_{31}Dy_{69}$ glass is a member of the transition metal-lanthanide or actinide (TM-LA) element group, while $Ni_{81}B_{19}$ is a candidate of the transition metal-metalloid (TM-M) glass. Another four metallic glasses such as $Ni_{33}Y_{67}$, $Ni_{36}Zr_{64}$, $Ni_{50}Zr_{50}$ and $Ni_{60}Nb_{40}$ are members of the transition metallic (TM-TM) glasses. The phonon dynamics of $Ni_{33}Y_{67}$ glass was studied by Arun Pratap et al. [1] using Hubbard-Beeby (HB) [3] and Takeno-Goda (TG) [4,5] approaches. The vibrational dynamics of $Ni_{50}Zr_{50}$ glass has been studied by Gupta et al. [2] using Takeno-Goda (TG) [4,5] and Bhatia-Singh (BS) [5] approaches. The phonon dynamics of $Ni_{31}Dy_{69}$, $Ni_{36}Zr_{64}$, $Ni_{60}Nb_{40}$ and $Ni_{81}B_{19}$ metallic glasses is not reported previously using model potential formalism. Recently, we have reported the vibrational properties of some binary metallic glasses [8–23].

Received March 25, 2011; accepted April 27, 2011
Humanities and Social Science Department, STBS College of Diploma Engineering, Surat 395 006, India
E-mail: voraam@yahoo.com

Looking to the advantages of metallic glasses, the present paper is emphasizing the phonon dynamics of six Ni-based amorphous alloys viz. $Ni_{31}Dy_{69}$, $Ni_{33}Y_{67}$, $Ni_{36}Zr_{64}$, $Ni_{50}Zr_{50}$, $Ni_{60}Nb_{40}$ and $Ni_{81}B_{19}$ using well recognized model potential [8–23]. The thermodynamics and elastic properties such as longitudinal sound velocity υ_L, transverse sound velocity υ_T, isothermal bulk modulus B_T, modulus of rigidity G, Poisson's ratio σ, Young's modulus Y and Debye temperature θ_D are computed from the elastic limit of the dispersion relation. Five different types of local field correction functions proposed by Hartree (H) [24], Taylor (T) [25], Ichimaru-Utsumi (IU) [26], Farid et al. (F) [27] and Sarkar et al. (S) [28] are used to study the exchange and correlation effects in the aforesaid studies. The phenomenological theory of Hubbard-Beeby [3] in the random phase approximation is employed to generate the phonon dispersion curves (PDC). The most important ingredient of the PDC is pair potential computed theoretically in Wills-Harrison (WH) [29] form from the well recognized model potential [8–23].

2 Theoretical methodology

The fundamental ingredient, which goes into the calculation of the phonon dynamics of metallic glasses, is the pair potential. In the present study, for TM-LA, TM-TM and TM-M metallic glasses, the pair potential is computed using [6–23,29],

$$V(r) = V_S(r) + V_b(r) + V_r(r) \tag{1}$$

The s-electron contribution to the pair potential $V_S(r)$ is calculated from [6–23]

$$V_S(r) = \frac{Z_S^2 e^2}{r} + \frac{\Omega_O}{\pi^2}\int F(q)\frac{\sin(qr)}{qr}\,q^2 dq \tag{2}$$

Here Z_S~1.5 is found by integrating the partial s-density of states resulting from self-consistent band structure calculation for the entire 3d and 4d series [29], while Ω_O is the effective atomic volume of the one component fluid.

The energy wave number characteristics appearing in Eq. (2) is written as [6–23,29]

$$F(q) = \frac{-\Omega_O q^2}{16\pi}|W_B(q)|^2\frac{\varepsilon_H(q)-1}{1+[\varepsilon_H(q)-1][1-f(q)]} \tag{3}$$

where, $W_B(q)$ is the effective bare ion potential, $\varepsilon_H(q)$ the Hartree dielectric response function [24] and $f(q)$ is the local field correction function to introduce the exchange and correlation effects.

The well recognized model potential $W_B(q)$ [8–23] used in the present computation of phonon dynamics of binary metallic glasses is of the form

$$W_B(q)=\frac{-4\pi e^2 Z}{\Omega_O q^2}\Bigg\{\Bigg[-1+\frac{12}{U^2}+\frac{U^2}{1+U^2}+\frac{6U^2}{(1+U^2)^2}+\frac{18U^2}{(1+U^2)^3}-\frac{6U^4}{(1+U^2)^3}+\frac{24U^2}{(1+U^2)^4}-\frac{24U^4}{(1+U^2)^4}\Bigg]\cdot\cos U+\Bigg[\frac{6}{U}-\frac{12}{U^3}+\frac{U}{1+U^2}+\frac{3U}{(1+U^2)^2}-\frac{3U^3}{(1+U^2)^2}+\frac{6U}{(1+U^2)^3}-\frac{18U^3}{(1+U^2)^3}+\frac{6U}{(1+U^2)^4}-\frac{36U^3}{(1+U^2)^4}+\frac{6U^5}{(1+U^2)^4}\Bigg]\sin U+24U^2\exp(1)\frac{U^2-1}{(1+U^2)^4}\Bigg\} \quad (4)$$

here $U=qr_C\cdot r_C$ is the model potential parameter. This form has the feature of a Coulombic term outside the core and varying cancellation due to repulsive and attractive contributions to the potential within the core in real space. The detailed information of this potential is given in the literature [8–23]. The model potential parameter r_C is calculated from the well known formula [8–23] as follows:

$$r_C=\frac{0.51r_S}{Z^{1/3}} \quad (5)$$

Here r_S is the Wigner-Seitz radius of the amorphous alloys.

The d-electron contributions to the pair potential are expressed in terms of the number of d-electron Z_d, the d-state radii r_d and the nearest-neighbor coordination number N_C as follows [29]:

$$V_b(r)=-Z_d\left(1-\frac{Z_d}{10}\right)\left(\frac{12}{N_C}\right)^{\frac{1}{2}}\frac{28.06}{\pi}\cdot\frac{2r_d^3}{r^5} \quad (6)$$

and

$$V_r(r)=Z_d\frac{450}{\pi^2}\cdot\frac{r_d^6}{r^8} \quad (7)$$

The theories of Hubbard-Beeby [3], Takeno-Goda [4,5] and Bhatia-Singh [6,7] have been employed in the present computation. The expressions for longitudinal phonon frequency ω_L and transverse phonon frequency ω_T as per HB, TG and BS approaches are given below [3–7].

According to the HB [3], the expressions for longitudinal phonon frequency ω_L and transverse phonon frequency ω_T are [3]

$$\omega_L^2(q)=\omega_E^2\left[1-\frac{\sin(q\sigma)}{q\sigma}-\frac{6\cos(q\sigma)}{(q\sigma)^2}+\frac{6\sin(q\sigma)}{(q\sigma)^3}\right] \quad (8)$$

and

$$\omega_T^2(q)=\omega_E^2\left[1-\frac{3\cos(q\sigma)}{(q\sigma)^2}+\frac{3\sin(q\sigma)}{(q\sigma)^3}\right] \quad (9)$$

with $\omega_E^2=\frac{4\pi\rho}{3M}\int_0^\infty g(r)V''(r)r^2\mathrm{d}r$ is the maximum frequency.

The theory for computing the phonon dynamics in amorphous solids, proposed by TG [4,5], has been employed in the present computation. The expressions for longitudinal phonon frequency ω_L and transverse phonon frequency ω_T as per TB approach are [4,5]

$$\omega_L^2(q)=\frac{4\pi\rho}{M}\int_0^\infty \mathrm{d}rg(r)\Bigg\{rV'(r)\left(1-\frac{\sin(qr)}{qr}\right)+[r^2V''(r)-rV'(r)]\left[\frac{1}{3}-\frac{\sin(qr)}{qr}-\frac{2\cos(qr)}{(qr)^2}+\frac{2\sin(qr)}{(qr)^3}\right]\Bigg\} \quad (10)$$

and

$$\omega_T^2(q)=\frac{4\pi\rho}{M}\int_0^\infty \mathrm{d}rg(r)\Bigg\{rV'(r)\left(1-\frac{\sin(qr)}{qr}\right)+[r^2V''(r)-rV'(r)]\left[\frac{1}{3}+\frac{2\cos(qr)}{(qr)^2}+\frac{2\sin(qr)}{(qr)^3}\right]\Bigg\} \quad (11)$$

Here M and ρ are the atomic mass and the number density of the glassy alloy, respectively, while $V''(r)$ is the second derivative of the pair potential.

Recently BS [6] was modified by Shukla and Campnaha [7]. They introduced screening effects in the BS approach. Then, with the above assumptions and modification, the dispersion equations for an amorphous material can be written as [6,7]

$$\rho\omega_L^2(q)=\frac{2N_C}{q^2}(\beta I_0+\delta I_2)+\frac{k_e k_{\mathrm{TF}}^2 q^2\varepsilon(q)|G(qr_S)|^2}{q^2+k_{\mathrm{TF}}^2\varepsilon(q)} \quad (12)$$

and

$$\rho\omega_T^2(q)=\frac{2N_C}{q^2}\left(\beta I_0+\frac{1}{2}\delta(I_0-I_2)\right) \quad (13)$$

The other details of used constants in the BS approach were already narrated in the literatures [23,24]. Here M is the effective atomic mass, ρ is the effective number density, and N_C is the effective coordination number of the glassy system.

In the long wavelength limit of the frequency spectrum, both phonon frequencies viz. the longitudinal ω_L and

transverse ω_T phonon frequencies are proportional to the wave vectors and obey the relationships [8–23]

$$\omega_L \propto q \text{ and } \omega_T \propto q,$$

$$\omega_L = v_L q \text{ and } \omega_T = v_T q \tag{14}$$

where, v_L and v_T are the longitudinal and transverse sound velocities of the glassy alloys, respectively. Detailed expressions of the long wavelength limit of the frequency spectrum are narrated in our earlier papers.

The present study also includes isothermal bulk modulus B_T, modulus of rigidity G, Poisson's ratio σ, Young's modulus Y and Debye temperature θ_D from the elastic limit of the PDC. All the quantities are computed from the longitudinal and transverse sound velocities (v_L and v_T). The bulk modulus B_T, modulus of rigidity G, Poisson's ratio σ, Young's modulus Y and Debye temperature θ_D are obtained using the expressions [3–23],

$$B_T = \rho_M \left(v_L^2 - \frac{4}{3} v_T^2 \right) \tag{15}$$

$$G = \rho_M v_T^2 \tag{16}$$

with ρ_M being the isotropic number density of the solid.

$$\sigma = \frac{1 - 2 \cdot \frac{v_T^2}{v_L^2}}{2 - 2 \cdot \frac{v_T^2}{v_L^2}} \tag{17}$$

$$Y = 2G(\sigma + 1) \tag{18}$$

and

$$\theta_D = \frac{\hbar \, \omega_D}{k_B} = \frac{\hbar}{k_B} 2\pi \left(\frac{9\rho}{4\pi} \right)^{\frac{1}{3}} \left(\frac{1}{v_L^3} + \frac{2}{v_T^3} \right)^{-\frac{1}{3}} \tag{19}$$

The low temperature specific heat C_V can be calculated from the following expressions [30],

$$C_V = \frac{\Omega_O \hbar^2}{k_B T^2} \sum_{\lambda = L,T} \int \frac{d^3 q}{(2\pi)^3} \frac{\omega_\lambda^2(q)}{\left[\exp\left(\frac{\hbar \omega_\lambda(q)}{k_B T} \right) - 1 \right] \left[1 - \exp\left(-\frac{\hbar \omega_\lambda(q)}{k_B T} \right) \right]} \tag{20}$$

Here, $\hbar$, k_B, and ω_D are the Plank's constant, Boltzmann's constant, and Debye frequency, respectively.

3 Results and discussion

The input parameters and other related constants used in the present computations are tabulated in Table 1, which are computed from the pure metallic data and taken from the literature [29].

Table 1 Input parameters and other constants

Glasses	Z	Ω_O/a.u.^{3}	r_C/a.u.	Z_d	N_C	r_d/a.u.
$Ni_{31}Dy_{69}$	2.69	158.44	0.8930	3.67	12.00	2.93
$Ni_{33}Y_{67}$	2.67	160.48	0.9028	3.81	12.00	2.44
$Ni_{36}Zr_{64}$	3.28	126.09	0.7189	4.66	12.00	2.19
$Ni_{50}Zr_{50}$	3.00	114.47	0.7384	5.50	12.00	2.00
$Ni_{60}Nb_{40}$	3.20	90.61	0.6632	6.50	10.40	1.77
$Ni_{81}B_{19}$	2.19	70.77	0.7835	7.08	11.43	1.28

The presently calculated pair potentials of $Ni_{31}Dy_{69}$ glass are shown in Fig. 1(a), which elucidates that the inclusion of screening functions hardly changes the nature of the pair potentials, except around the first minimum. The well depth slightly increases due to the influence of various screening functions compared to H-screening. The presently obtained pair potentials of $Ni_{33}Y_{67}$ glass are shown in Fig. 1(b) along with the other such theoretical results [1,23]. The first zero position of pair potentials at $r = r_0$ under all screening functions occurs at $r_0 \approx 3.95$ a.u.. Thus, the inclusion of exchange and correlations on the $V(r = r_0)$ is not substantial. But the well width increases compared to H-screening. It is observed that the well depth of presently computed pair potentials shifted towards the left and were as high as compared to the results of Arun Pratap et al. [1] and Hausleitner-Hafner [31]. The presently generated pair potentials of $Ni_{36}Zr_{64}$ glass are displayed in Fig. 1(c). The first zero for $V(r = r_0)$ under all screening functions occurs at $r_0 \approx$ 3.74 a.u.. The maximum depth in the pair potentials is obtained for *S*-function. The pair potentials under remaining *T*, *IU* and *F*-screening functions are lying between those under *H* and *S*-screening function. The presently calculated pair potentials of $Ni_{50}Zr_{50}$ glass are observed in Fig. 1(d) along with the other such available theoretical data [2,32]. The position of pair potentials at $r = r_0$ under *H*-function occurs at r_0 = 3.62 a.u., while the influence of screenings suppresses this zero slightly and makes it occur at $r_0 \leqslant 3.55$ a.u.. The broad well width is seen due to the inclusion of local field correction functions. It is seen that the well depth of presently computed pair potentials shifted towards the left and were as high as compare to the outcomes of Gupta et al. [2] and Hausleitner-Hafner [32]. The computed pair potentials of $Ni_{60}Nb_{40}$ glass are displayed in Fig. 1(e). It is apparent from the behavior that the inclusion of screening effects increases the well width slightly compared to H–screening. The first zero for $V(r = r_0)$ under H occurs at r_0 = 3.38 a.u., while the inclusion of exchange and correlations suppresses this zero to $r_0 \leqslant 3.28$ a.u.. The pair potentials of the two components of $Ni_{81}B_{19}$ glass are shown in Fig. 1(f). It is noticed that the first

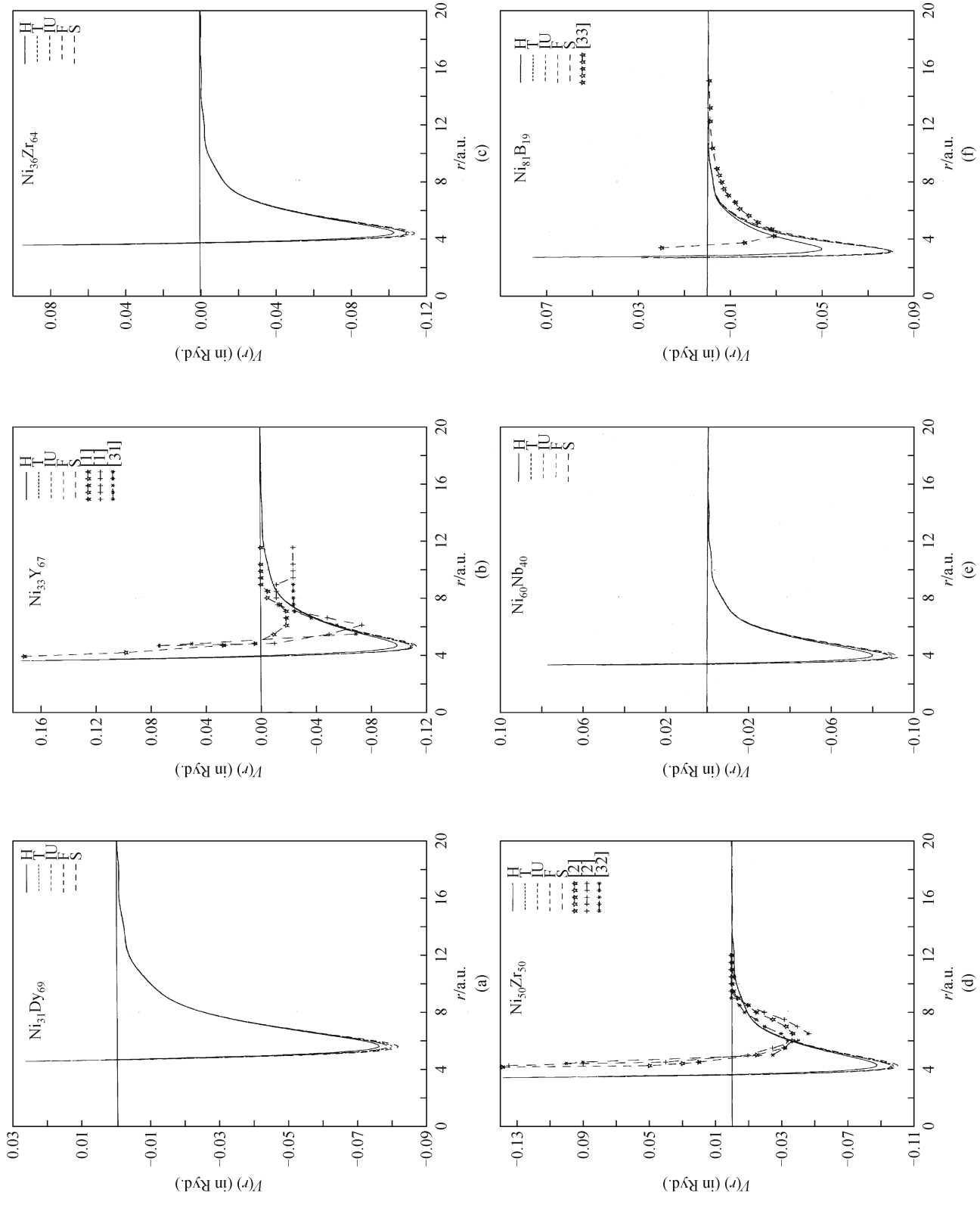

Figure 1 Pair potentials for (a) $Ni_{31}Dy_{69}$, (b) $Ni_{33}Y_{67}$, (c) $Ni_{36}Zr_{64}$, (d) $Ni_{50}Zr_{50}$, (e) $Ni_{60}Nb_{40}$ and (f) $Ni_{60}Nb_{40}$ metallic glasses

zero for $V(r = r_0)$ under all local field correction functions occurs around $r_0 \approx 3.26$ a.u.. The well width also increases with respect to H-screening. The position of $V_{\min}(r)$ is affected by the nature of the screenings. It is observed that the well depth of presently computed potentials move towards the left as compared to that of Hausleitner and Hafner [33]. The present results of the pair potentials of all the Ni-based amorphous alloys do not show any oscillatory behavior and are almost constant in the large *r*-region. The presently computed pair potentials from *H*, *T*, *IU*, *F* and *S*-local field correction functions for most of the amorphous alloys are overlapped with each other.

The pair potentials for the six Ni-based amorphous alloys computed using *S*-local field correction function is displayed in Fig. 2. In this figure, we have compared our presently computed pair potentials from *S*-local field correction function with each other for most of the amorphous alloys. This figure indicates the shifting of the pair potentials with respect to atomic volume Ω_O of the amorphous alloys. The repulsive coulomb interaction and the attractive interactions represented by oscillatory nature are observed. It is also noticed that when volume Ω_O of the glassy alloys increases (Ω_O is more for $Ni_{33}Y_{67}$ glass), the potential depth rises. It means that the pair potential for $Ni_{33}Y_{67}$ glass shows higher depth in comparison with other metallic glasses. The potential well width of $Ni_{81}B_{19}$ glass shifts at lower *r* -values, while that of $Ni_{31}Dy_{69}$ glass shifts at higher *r* -values. The lanthanide element Dy and metalloid component B plays an important role in the nature of the pair potentials of respective amorphous alloys, i.e., for $Ni_{31}Dy_{69}$ glass, the repulsive interaction is more in composition with $Ni_{81}B_{19}$ metallic glass. All the pair potentials show the combined effect of the *s*- and *d*-electrons. Bretonnet and Derouiche [34] observed that the repulsive part of $V(r)$ is drawn lower and its attractive part is deeper due to the *d*-electron effect. When we go from $Ni_{31}Dy_{69} \rightarrow Ni_{81}B_{19}$, the net number of *d*-electron r_d decreases, hence the $V(r)$ is shifted towards the lower *r*-values. Therefore, the present results have supported the *d*-electron effect as noted by Bretonnet and Derouiche [34].

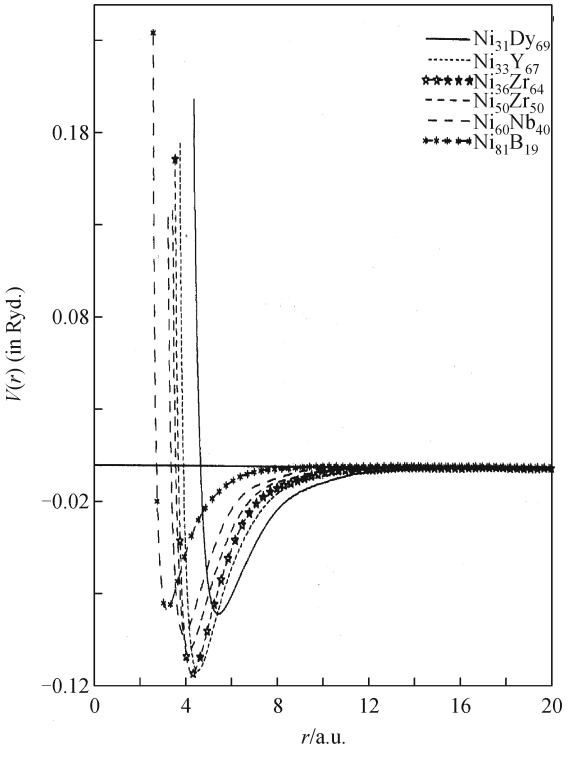

Figure 2 Pair potentials for $Ni_{31}Dy_{69}$, $Ni_{33}Y_{67}$, $Ni_{36}Zr_{64}$, $Ni_{50}Zr_{50}$, $Ni_{60}Nb_{40}$ and $Ni_{60}Nb_{40}$ metallic glasses using S-local field correction function

From Figs. 1 and 2, it is noted that the Coulomb repulsive potential part dominates the oscillations due to ion-electron-ion interactions, which shows the waving shape oscillation of the potential after $r \approx 10$ a.u.. Hence, the pair potentials converge towards a finite value instead of zero in repulsive region.

The phonon modes for longitudinal and transverse branches of $Ni_{31}Dy_{69}$, $Ni_{33}Y_{67}$, $Ni_{36}Zr_{64}$, $Ni_{50}Zr_{50}$, $Ni_{60}Nb_{40}$ and $Ni_{81}B_{19}$ metallic glasses calculated using HB approach with the five screening functions are shown in Figs. 3–8. The phonon eigen frequencies of $Ni_{31}Dy_{69}$ glass calculated using HB approach to study the screening influence are shown in Fig. 3. From this figure, it is seen that the present results of phonon modes due to *H*, *T* and *F*-function are lying between those due to *IU* and *S*-screenings. The first minimum in the longitudinal branch is found around 1.72 $Å^{-1}$ for H, 2.36 $Å^{-1}$ for *T* and *IU*, 2.52 $Å^{-1}$ for *F* and *S*-local field correction functions. The influence of *T*, *IU* and *F* on ω_L is ranging from 7.9% to 11%. The *S*-function enhances the ω_L of $Ni_{31}Dy_{69}$ glass by $\approx$ 67.8% in comparison to *H*-dielectric function. At $q \approx 1.0$ $Å^{-1}$ point, the influence of various local field correction functions on ω_T due to *T*, *IU*, *F* and *S*-screening is 19.98%, 22.03%, 20.27% and 35.99%, respectively. From Fig. 4, it is noted that the present results of PDC of $Ni_{33}Y_{67}$ glass due to *T*, *IU* and *F* are lying between those due to *S* and *H*-screening. The present results are found to be qualitatively in agreement with the available theoretical data [1]. The first depth in the longitudinal branch is observed around 1.75 $Å^{-1}$ for *H*, 2.62 $Å^{-1}$ for *T* and *IU*, 2.51 $Å^{-1}$ for *F* and 1.74 $Å^{-1}$ for *S*-function. The screening influence on the first maximum of ω_L for *T* is 47.78%, for *IU* is 36.18%, for *F* is 46.06% and for *S*-screening is 43.14% with respect to *H*-screening, which does not include any exchange and correlation effects. At $q \approx 1.0$ $Å^{-1}$ point, the influence on ω_T due to *T*, *IU*, *F* and *S*-exchange and correlation functions is 2.75%, 17.78%, 1.15% and 15.55%, respectively, in comparison with *H*-dielectric function. From Fig. 5, it is evident that

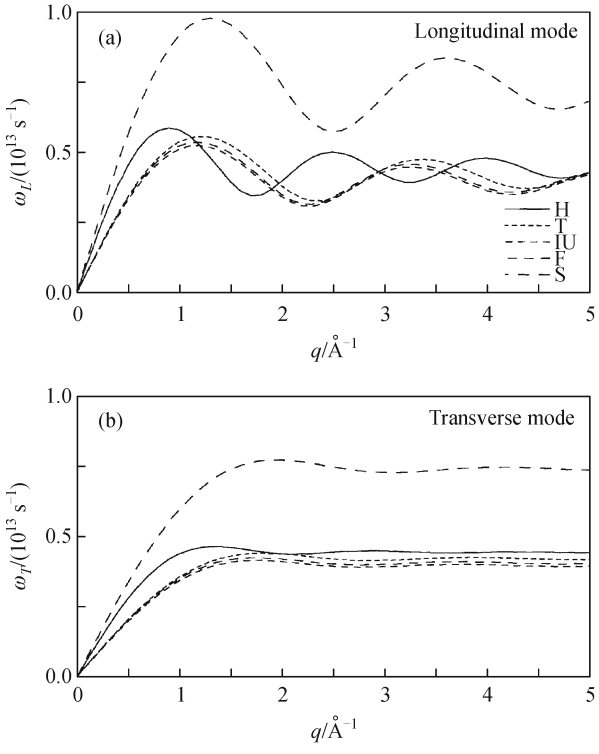

Figure 3 Phonon dispersion curves for $Ni_{31}Dy_{69}$ metallic glasses

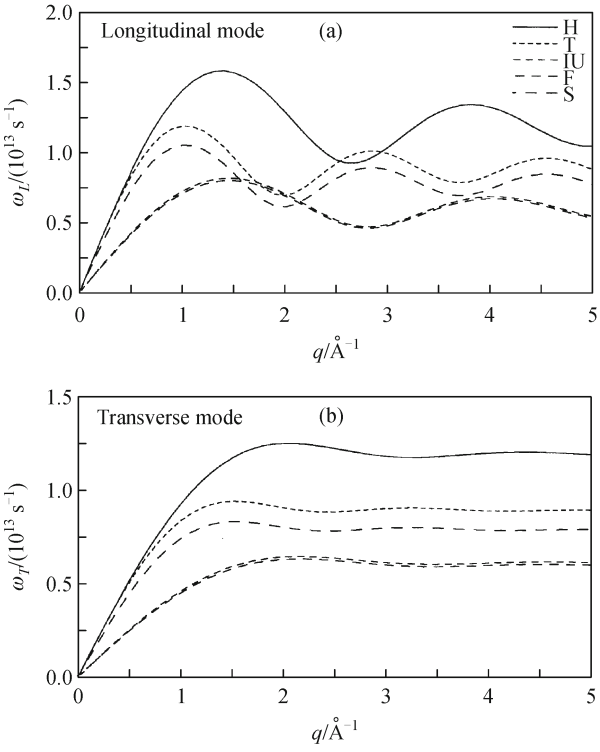

Figure 5 Phonon dispersion curves for $Ni_{36}Zr_{64}$ metallic glasses

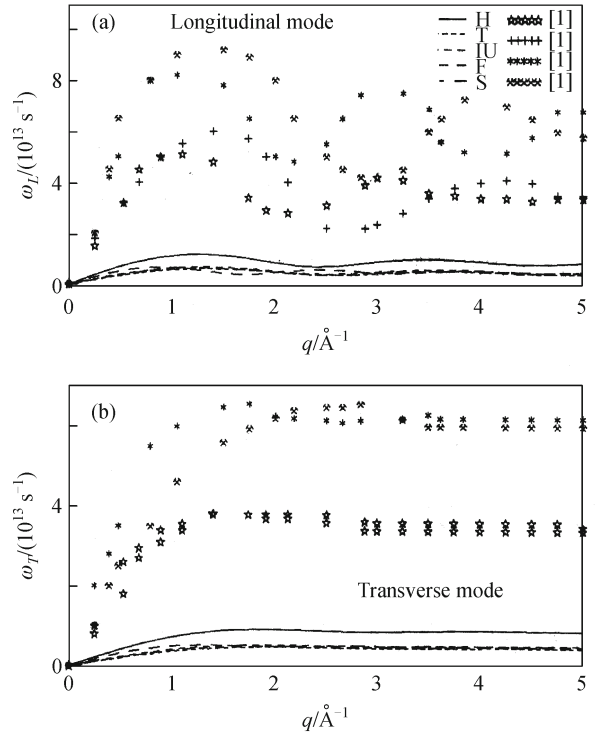

Figure 4 Phonon dispersion curves for $Ni_{33}Y_{67}$ metallic glasses

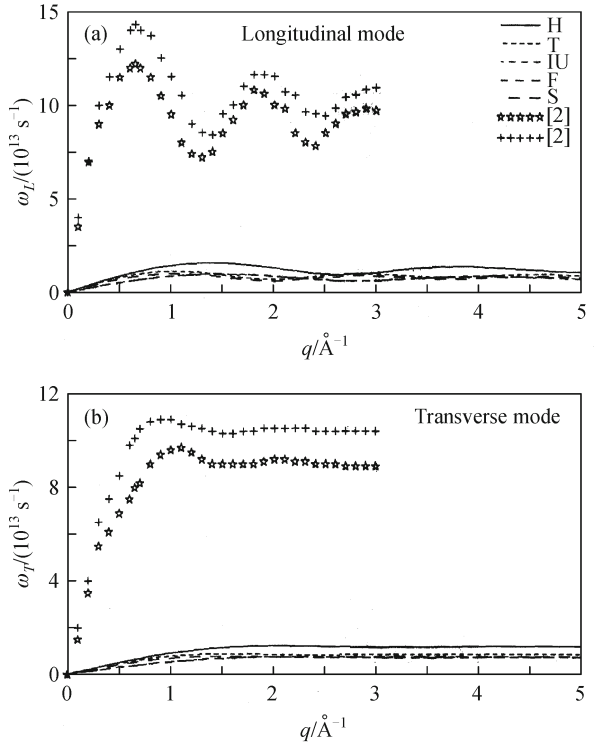

Figure 6 Phonon dispersion curves for $Ni_{50}Zr_{50}$ metallic glasses

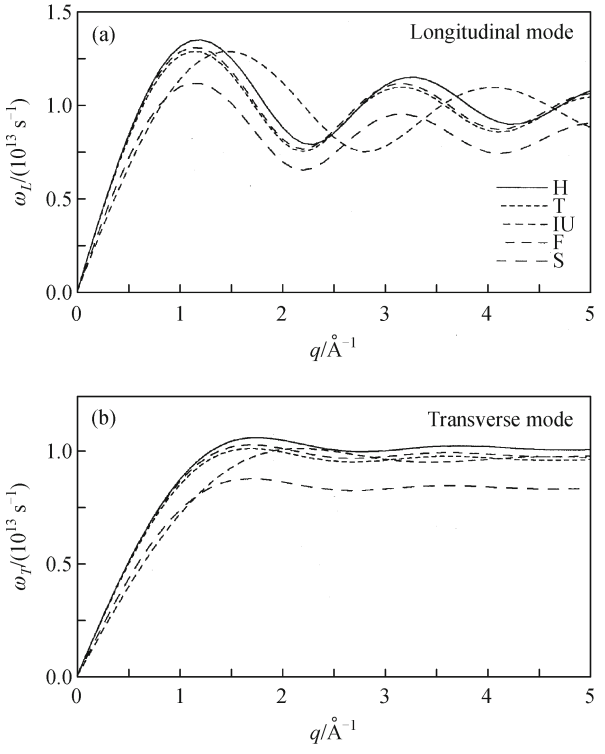

Figure 7 Phonon dispersion curves for $Ni_{60}Nb_{40}$ metallic glasses

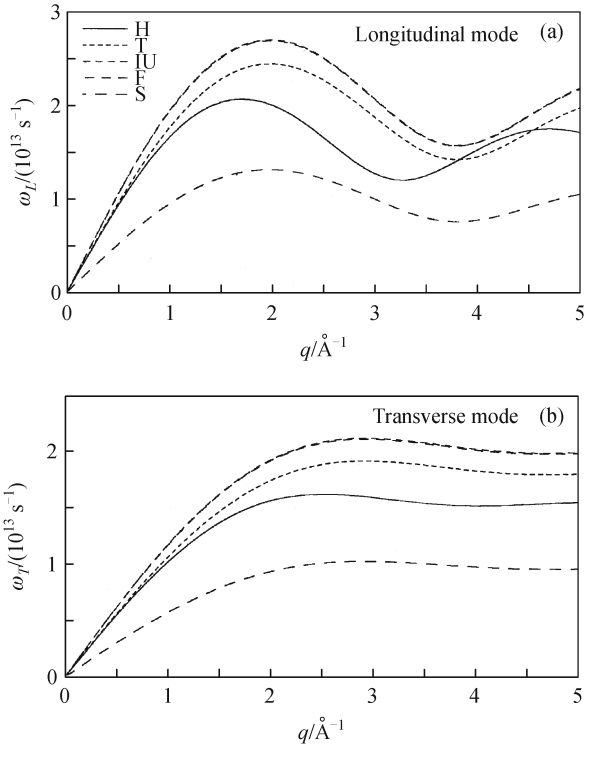

Figure 8 Phonon dispersion curves for $Ni_{60}Nb_{40}$ metallic glasses

the inclusion of exchange and correlation effects suppresses the phonon frequencies of $Ni_{36}Zr_{64}$ glass. The first depth in the longitudinal branch is found around 2.72 $Å^{-1}$ for *H*, 2.03 $Å^{-1}$ for *T*, 2.85 $Å^{-1}$ for *IU* as well as for *F* and 2.02 $Å^{-1}$ for *S*-screening function. The effect of *T*, *IU*, *F* and *S*-screening at first maximum of ω_L is about 24.91%, 67.28%, 49.49% and 33.56%, respectively, in comparison to static *H*-dielectric function. The screening effects observed at $q \approx 1.0\ Å^{-1}$ position in transverse branch for *T*, *IU*, *F* and *S*-functions is 9.72%, 50.47%, 51.52% and 20.18%, respectively. It is noticed from Fig. 6 that the inclusion of exchange and correlation effects suppresses the longitudinal as well as transverse phonon branches of $Ni_{50}Zr_{50}$ glass. The present results are found to be qualitatively in agreement with the available theoretical data [2]. The first depth in the longitudinal branch for *H*, *T*, *IU*, *F* and *S*-local field correction functions lies at $q \approx 2.72\ Å^{-1}$, 2.13 $Å^{-1}$, 2.85 $Å^{-1}$, 2.84 $Å^{-1}$ and 2.03 $Å^{-1}$, respectively. The screening influences at the first peak of ω_L with respect to *H*-screening are 14.73% for *T*, 38.46% for *IU*, 39.50% for *F* and 37.08% for *S*-screening. Such influences on ω_T at $q \approx 1.0\ Å^{-1}$ for *T* is 14.17%, for *IU* is 41.10%, for *F* is 42.11% and for *S*-screening is 24.21%. It is evident from Fig. 7 that the height of the first peak and the position of the first peak in the longitudinal and transverse modes of $Ni_{60}Nb_{40}$ glass are appreciably influenced by different screenings. The first minimum in the longitudinal branch for *H*, *T*, *IU*, *F* and *S*-local field correction functions occurs at $q \approx 2.32\ Å^{-1}$, 2.22 $Å^{-1}$, 2.21 $Å^{-1}$, 2.36 $Å^{-1}$ and 2.05 $Å^{-1}$, respectively. The effect of the *T*-screening at the first peak of ω_L is 3.65% with respect to *H*-function. Such effect of *IU*, *F* and *S*-function is 3.65%, 2.10% and 16.44%, respectively. The screening influence on ω_T at $q \approx 1.0\ Å^{-1}$ point due to *T*-dielectric function is 2.71%, due to *IU* is 17.75%, due to *F*-function is 1.10% and due to *S* is 15.58% with respect to *H*-dielectric function. It is seen from Fig. 8 that the inclusion of exchange and correlation effects enhances the phonon frequencies of $Ni_{81}B_{19}$ glass in longitudinal as well as transverse branches except for $f(q)$ of *S*-function. The first minimum in the longitudinal branch for *H*, *T*, *IU*, *F* and *S*-local field correction functions is around $q \approx 3.35\ Å^{-1}$, 3.32 $Å^{-1}$, 3.31 $Å^{-1}$, 3.34 $Å^{-1}$ and 3.45 $Å^{-1}$, respectively. At the first maximum, the screening influences on ω_L is 0.48% to 11.25% with respect to static *H*-screening, while such influence on ω_T at $q \approx 1.0\ Å^{-1}$ point is about 14.78% to 63.10%.

The PDC calculated from the HB, TG and BS approaches with *S*-local field correction function of $Ni_{31}Dy_{69}$, $Ni_{33}Y_{67}$, $Ni_{36}Zr_{64}$, $Ni_{50}Zr_{50}$, $Ni_{60}Nb_{40}$ and $Ni_{81}B_{19}$ metallic glasses are shown in Figs. 9(a)–(f). The first minimum in the longitudinal branch of $Ni_{31}Dy_{69}$ metallic glass falls at $q \approx 1.8\ Å^{-1}$ for BS, 2.7 $Å^{-1}$ for TG and 2.6 $Å^{-1}$ for HB approach. The first minimum in the longitudinal branch of $Ni_{33}Y_{67}$ metallic glass

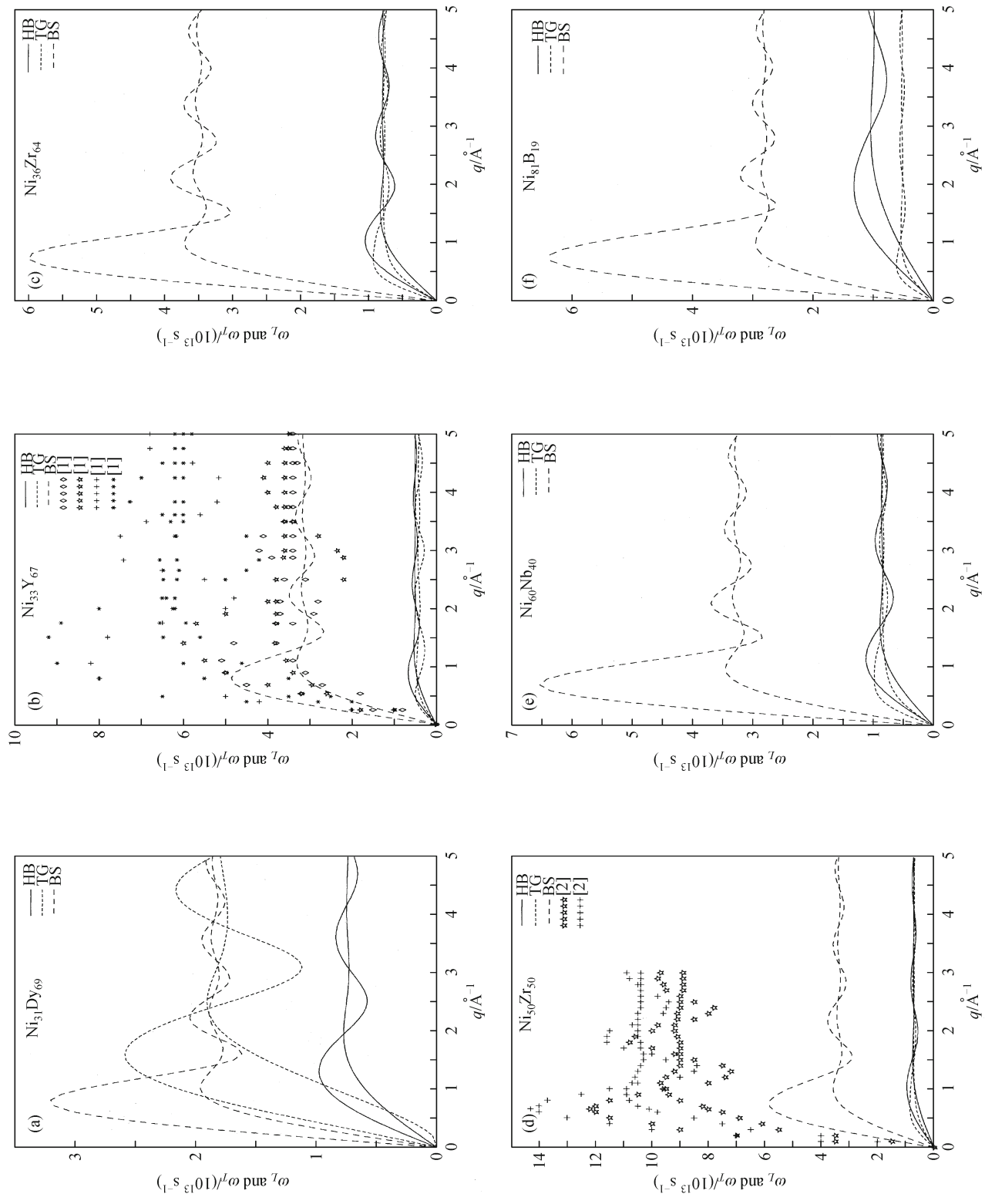

Figure 9 Screening dependence of phonon dispersion curves for (a) $Ni_{31}Dy_{69}$, (b) $Ni_{33}Y_{67}$, (c) $Ni_{36}Zr_{64}$, (d) $Ni_{50}Zr_{50}$, (e) $Ni_{60}Nb_{40}$ and (f) $Ni_{60}Nb_{40}$ metallic glasses computed from HB approach.

falls at 1.7 Å^{-1} for BS, 1.3 Å^{-1} for TG and1.6 Å^{-1} for HB approach. The first minimum in the longitudinal branch of $Ni_{36}Zr_{64}$ metallic glass falls at $q \approx 1.6$ Å^{-1} for BS, $q \approx 2.0$ Å^{-1} for TG and HB approaches. The first minimum in the longitudinal branch of $Ni_{50}Zr_{50}$ metallic glass occurs at $q \approx 2.0$ Å^{-1} for HB and TG approaches and $q \approx 2.0$ Å^{-1} for BS approach. The first minimum in the longitudinal branch of $Ni_{60}Nb_{40}$ metallic glass for HB and TG approaches falls at $q \approx 2.2$ Å^{-1} and for BS at $q \approx 1.6$ Å^{-1}. The first minimum in the longitudinal branch of $Ni_{81}B_{19}$ metallic glass occurs for HB, TG and BS approaches at $q \approx 3.4$ Å^{-1}, 3.6 Å^{-1} and 1.6 Å^{-1}, respectively. The first crossing position of ω_L and ω_T for $Ni_{81}B_{19}$ metallic glass in the HB, TG and BS approaches is seen at $q \approx 3.4$ Å^{-1}, 3.6 Å^{-1} and 1.6 Å^{-1}, respectively. The first crossing position of ω_L and ω_T for $Ni_{33}Y_{67}$ metallic glass in the HB, TG and BS approaches is seen at $q \approx 1.3$ Å^{-1}, 0.7 Å^{-1} and 1.2 Å^{-1}, respectively. The first crossing position of ω_L and ω_T for $Ni_{36}Zr_{64}$ metallic glass in the HB, TG and BS approaches is seen at $q \approx 11.5$ Å^{-1}, 1.5 Å^{-1} and 1.1 Å^{-1}, respectively. The first crossing position of ω_L and ω_T for $Ni_{50}Zr_{50}$ metallic glass in the HB, TG and BS approaches is seen at $q \approx 1.5$ Å^{-1}, 1.5 Å^{-1} and 1.3 Å^{-1}, respectively. The first crossover position of ω_L and ω_T for $Ni_{60}Nb_{40}$ metallic glass in the HB, TG and BS approaches is observed at $q \approx 1.7$ Å^{-1}, 1.6 Å^{-1} and 1.1 Å^{-1}, respectively. The first crossing point between two phonon frequencies, ω_L and ω_T, in the HB, TG and BS approaches for $Ni_{81}B_{19}$ metallic glass is observed at $q \approx 2.9$ Å^{-1}, 1.1 Å^{-1} and 1.5 Å^{-1}, respectively. Moreover, the present outcome of PDC with BS approach is higher than those with HB and TG approaches. The present results of PDC for $Ni_{33}Y_{67}$ and $Ni_{50}Zr_{50}$ binary metallic glasses are found to be qualitatively in agreement with the available theoretical data [1,2].

The results for the PDC obtained from HB approach using the *S*-local field correction function are shown in Fig. 10. It is observed from Fig. 10 that, the first peak position of longitudinal branch of $Ni_{31}Dy_{69}$ glass is higher, while that of $Ni_{33}Y_{67}$ glass is lower in comparison with other metallic glasses. Also the first minima of longitudinal branch of $Ni_{81}B_{19}$ glass shows at higher q-values, while it shows for $Ni_{33}Y_{67}$ glass at lower q-values. The lower dip in the longitudinal branch justifies the correctness and stability of the pair potential. The same results are observed in transverse branch as well. Moreover, it is observed from Fig. 10 that, the oscillations are more prominent in the longitudinal phonon modes as compared to the transverse modes. This shows the existence of collective excitations at larger momentum transfer due to longitudinal phonons only and the instability of the transverse phonons due to the anharmonicity of the atomic vibrations in the metallic systems. Also in the high wave vector region, damping of phonons dominates the transverse mode, which is indicating the fluid characteristic of the glass, i.e., the transverse phonon behavior is monotonic. Here in transverse branch, the frequencies increase with the wave vector q and then saturate at $\approx q = 2.0$ Å^{-1}, supporting the well known Thorpe model [35] that describes a glass like a solid containing finite liquid cluster. The transverse phonons are absorbed for frequencies larger than the smallest eigen frequencies of the largest cluster.

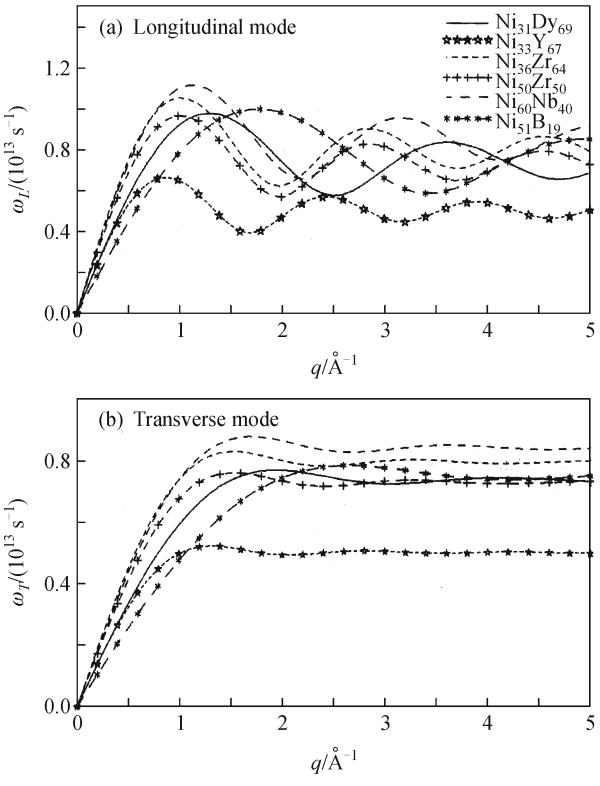

Figure 10 Phonon dispersion curves for (a) $Ni_{31}Dy_{69}$, (b) $Ni_{33}Y_{67}$, (c) $Ni_{36}Zr_{64}$, (d) $Ni_{50}Zr_{50}$, (e) $Ni_{60}Nb_{40}$ and (f) $Ni_{60}Nb_{40}$ metallic glasses computed from HB, TG and BS approaches using S-local field correction function

As shown in Figs. 11–16 for $Ni_{31}Dy_{69}$, $Ni_{33}Y_{67}$, $Ni_{36}Zr_{64}$, $Ni_{50}Zr_{50}$, $Ni_{60}Nb_{40}$ and $Ni_{81}B_{19}$ metallic glasses, the exchange and correlation functions also affected the anomalous behavior (i.e. deviation from the T^3 law), which is observed in the vibrational part of the low temperature specific heat C_V. The reason behind the anomalous behavior may be that the low frequency modes modify the generalized vibrational density of states of the glass with that of the polycrystal. These modes are mainly responsible for the difference in the temperature dependence of the vibrational part of the specific heat which departs from the normal behavior. The existence of a portion of the spectrum with 'softer phonons' (resembling rotons in liquid helium) may be the cause of anomalous behavior of low temperature specific heat C_V. In the low temperature region, a contribution to the

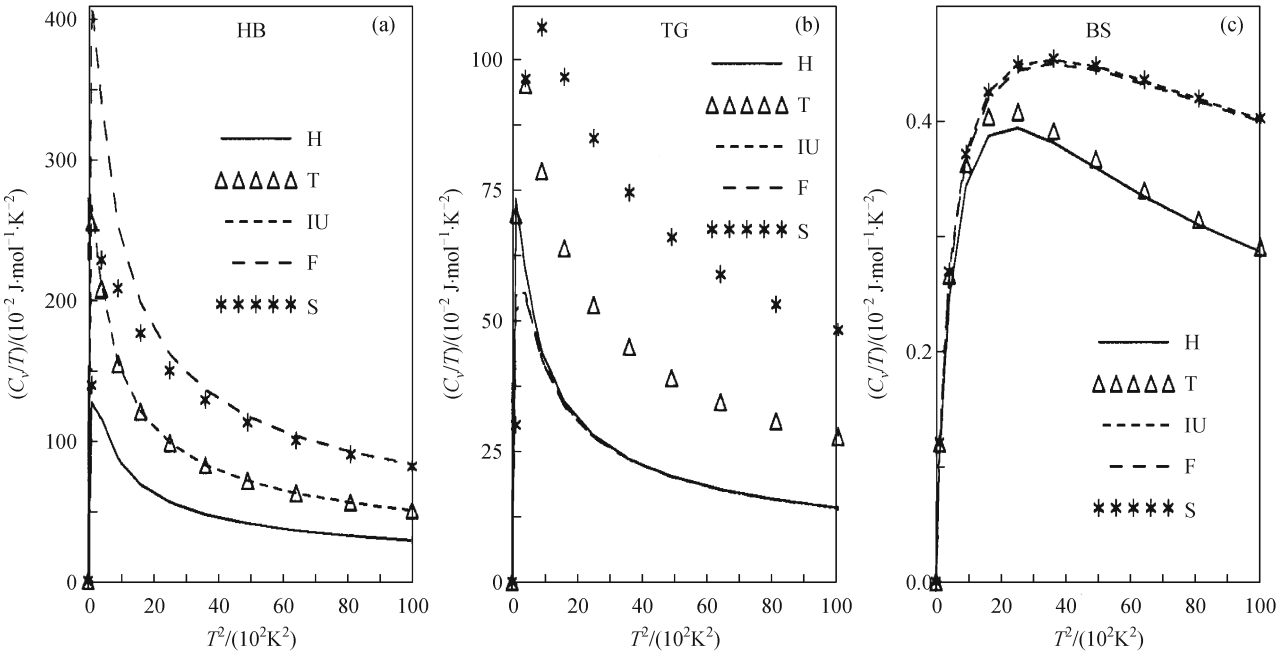

Figure 11 Screening dependence of the low temperature specific heat for $Ni_{31}Dy_{69}$ metallic glasses computed from HB, TG and BS approaches

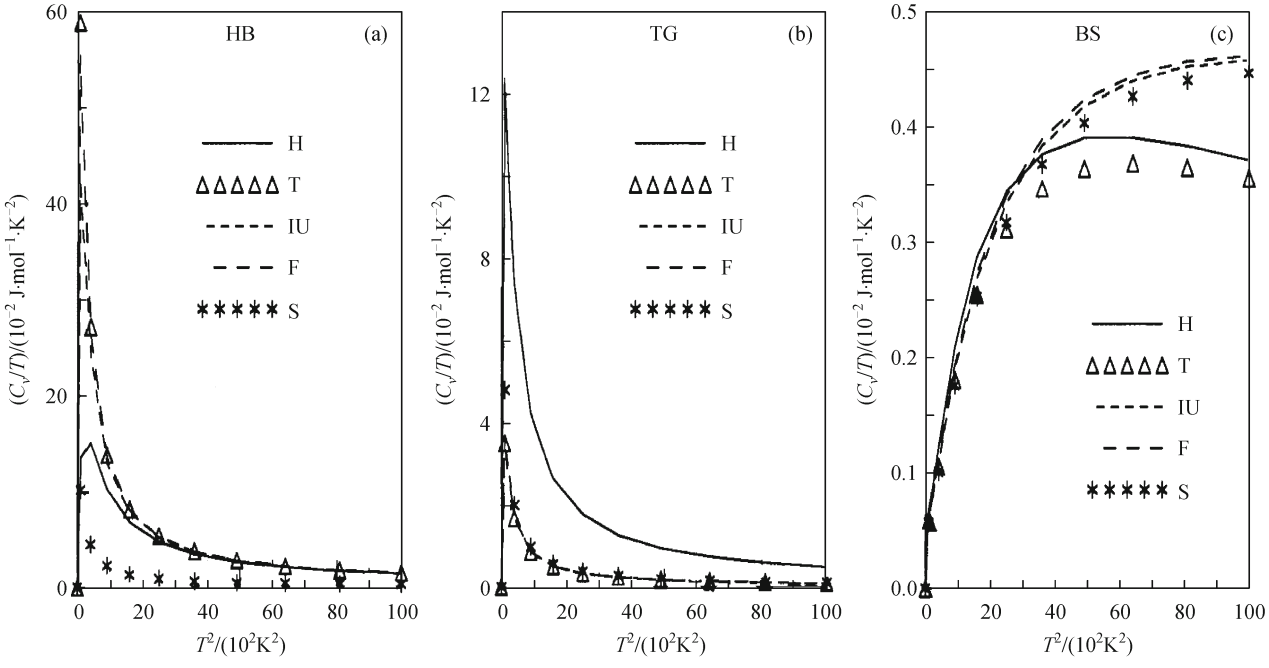

Figure 12 Screening dependence of the low temperature specific heat for $Ni_{33}Y_{67}$ metallic glasses computed from HB, TG and BS approaches

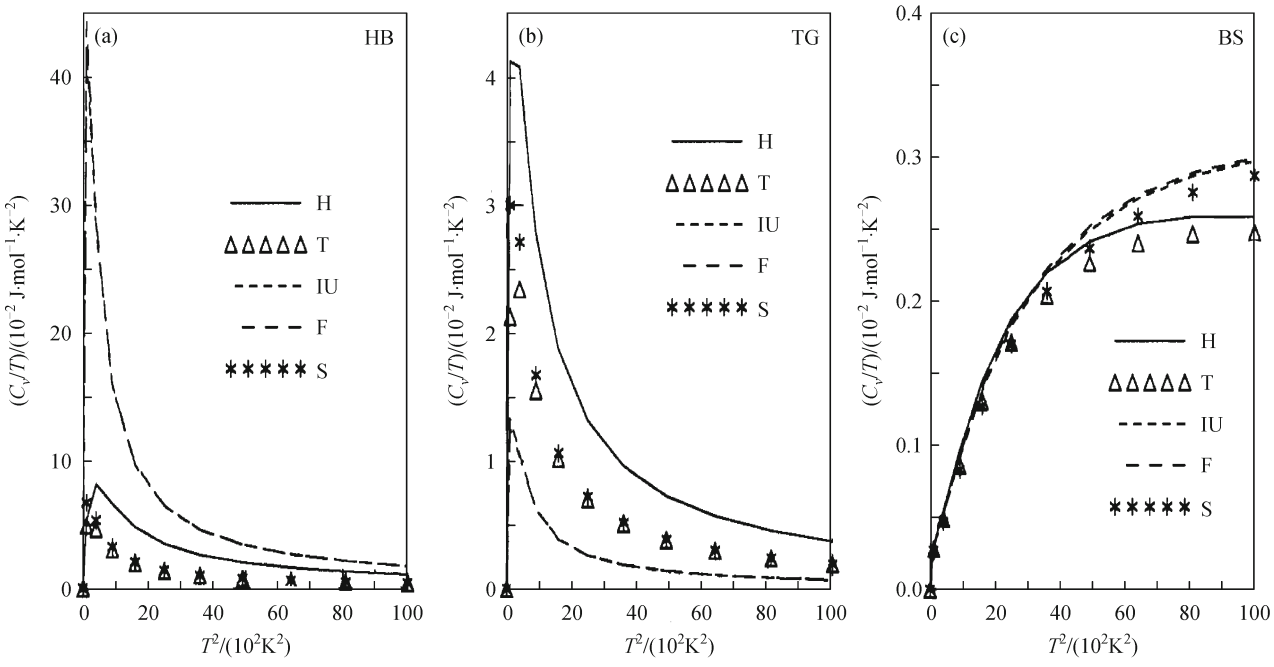

Figure 13 Screening dependence of the low temperature specific heat for $Ni_{36}Zr_{64}$ metallic glasses computed from HB, TG and BS approaches

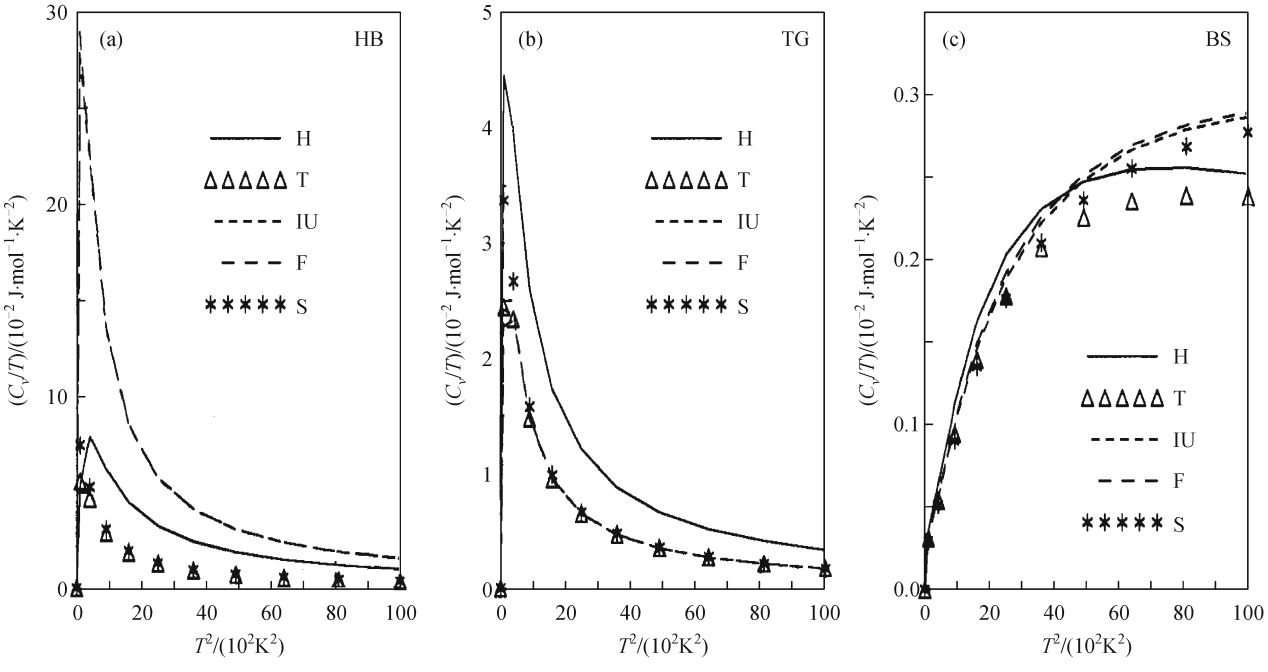

Figure 14 Screening dependence of the low temperature specific heat for $Ni_{50}Zr_{50}$ metallic glasses computed from HB, TG and BS approaches

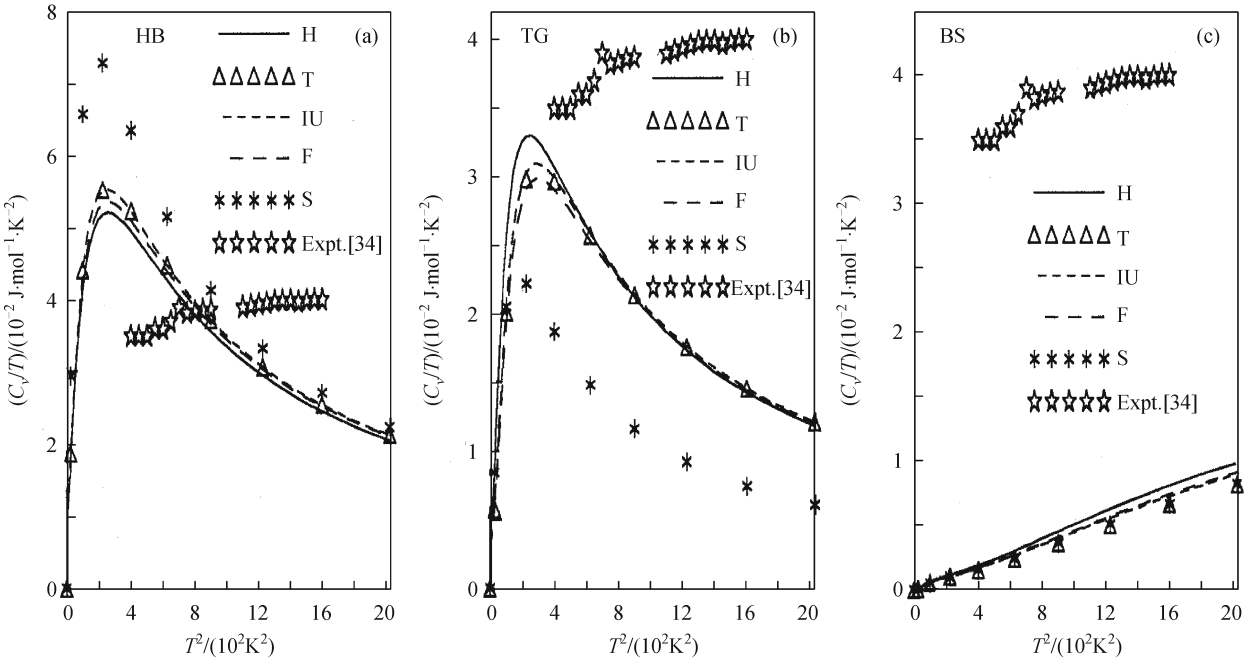

Figure 15 Screening dependence of the low temperature specific heat for $Ni_{60}Nb_{40}$ metallic glasses computed from HB, TG and BS approaches

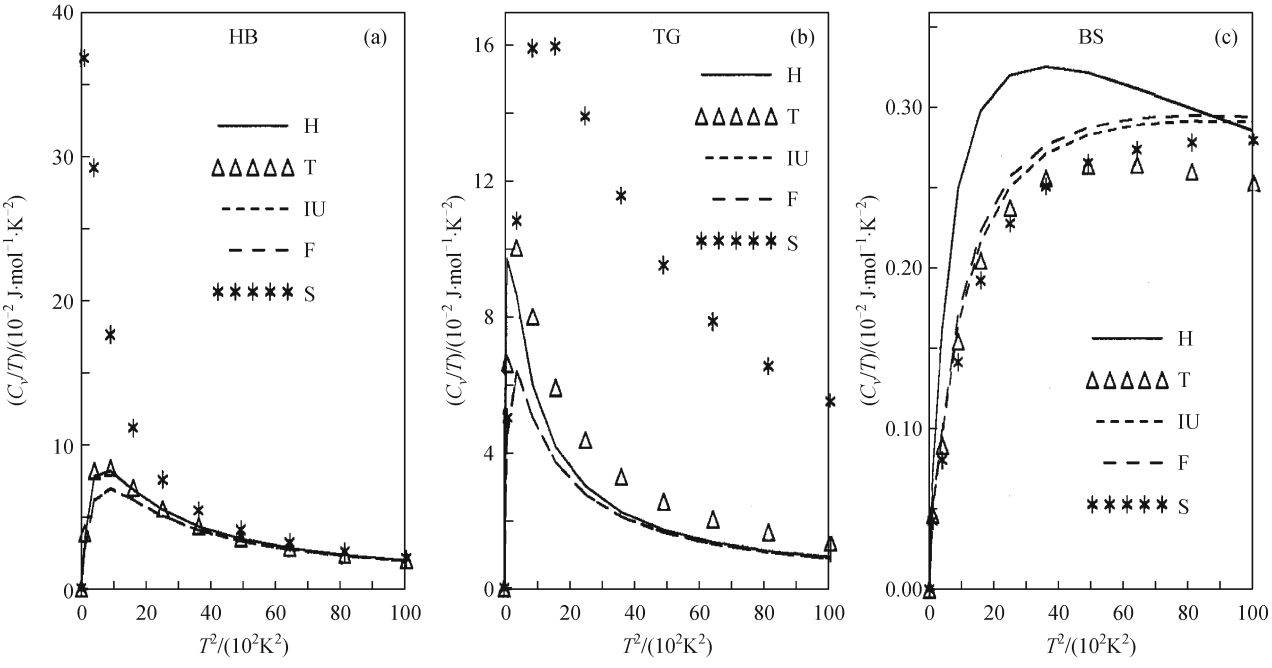

Figure 16 Screening dependence of the low temperature specific heat for $Ni_{60}Nb_{40}$ metallic glasses computed from HB, TG and BS approaches

low temperature specific heat C_V is made by phonons of the initial part of the frequency spectrum. When the temperature reaches a value at which the energy of the thermal motions becomes comparable to the energy of 'softer phonons' minimum, an additional contribution appears to heat capacity from the roton portion of the phonon frequency $\omega(q)$. The present results of low temperature specific heat for $Ni_{60}Nb_{40}$ binary metallic glass are found to be qualitatively in agreement with the available theoretical data [36].

Furthermore, the thermodynamic and elastic properties of Ni-based amorphous alloys estimated from the elastic limit of the PDC are tabulated in Tables 2–7. The present results of $Ni_{33}Y_{67}$ glass are found lower in line with other theoretical data [1]. Also the present outcome of $Ni_{50}Zr_{50}$ glass shows lower results in comparison with the theoretical reported data [2]. It is seen that the screening theory plays an important role in the prediction of the thermodynamic and elastic properties of metallic glasses. The present values of the isothermal bulk modulus B_T change with the atomic volume of binary metallic glass, which shows close similarity in the response of crystalline and disordered structures to compressive stains. The present results of sound velocities of $Ni_{33}Y_{67}$ and $Ni_{50}Zr_{50}$ binary metallic glasses are more than five and nine times lower than the highest theoretical data [1,2]. The

Table 2 Thermodynamic and elastic properties of amorphous $Ni_{31}Dy_{69}$ metallic glass

App.	SCR	$v_L/(10^3\ m\cdot s^{-1})$	$v_T/(10^3\ m\cdot s^{-1})$	$B_T/(10^9\ N\cdot m^{-2})$	$G/(10^9\ N\cdot m^{-2})$	σ	$Y/(10^9\ N\cdot m^{-2})$	θ_D/K
	H	1.0399	0.6004	0.5535	0.3321	0.2499	0.8303	69.33
	T	0.7308	0.4219	0.2734	0.1640	0.2500	0.4101	48.72
HB	IU	0.7113	0.4107	0.2590	0.1554	0.2499	0.3886	47.43
	F	0.7273	0.4199	0.2708	0.1625	0.2500	0.4062	48.50
	S	1.1986	0.6920	0.7354	0.4412	0.2500	1.1031	79.92
	H	1.3472	0.7310	1.0158	0.4924	0.2914	1.2717	84.84
	T	1.6901	1.1431	1.0267	1.2041	0.0784	2.5970	129.75
TG	IU	1.5785	1.0034	1.0590	0.9277	0.1610	2.1540	114.76
	F	1.6201	1.0360	1.1000	0.9889	0.1541	2.2827	118.41
	S	1.9934	1.4497	1.0793	1.9365	−0.0614	3.6353	162.79
	H	4.5340	2.2334	12.8138	4.5963	0.3398	12.3163	260.85
	T	4.4138	2.1908	12.0544	4.4226	0.3365	11.8221	255.77
BS	IU	4.4149	2.1740	12.1531	4.3550	0.3399	11.6710	253.92
	F	4.4415	2.1876	12.2975	4.4096	0.3399	11.8165	255.50
	S	4.3821	2.1867	11.8197	4.4059	0.3342	11.7569	255.20

Table 3 Thermodynamic and elastic properties of amorphous $Ni_{33}Y_{67}$ metallic glass

App.	SCR	$v_L/(10^3\ m\cdot s^{-1})$	$vT/(10^3\ m\cdot s^{-1})$	$B_T/(10^9\ N\cdot m^{-2})$	$G/(10^9\ N\cdot m^{-2})$	σ	$Y/(10^9\ N\cdot m^{-2})$	θ_D/K
	H	1.4852	0.8575	0.6753	0.4052	0.2499	1.0129	98.60
	T	0.7349	0.4243	0.1653	0.0992	0.2499	0.2480	48.79
HB	IU	0.8296	0.4790	0.2107	0.1264	0.2499	0.3160	55.08
	F	0.7726	0.4460	0.1827	0.1096	0.2501	0.2741	51.29
	S	1.2073	0.6970	0.4462	0.2677	0.2500	0.6693	80.16
	H	1.9854	0.8849	1.5967	0.4315	0.3760	1.1875	103.42
	T	1.9245	1.1303	1.1022	0.7040	0.2367	1.7414	129.78
TG	IU	1.8954	1.1068	1.0797	0.6750	0.2413	1.6758	127.15
	F	1.9390	1.1335	1.1279	0.7080	0.2404	1.7565	130.20
	S	1.6075	0.9926	0.7001	0.5429	0.1919	1.2942	113.41
	H	6.2959	3.3499	13.5977	6.1838	0.3025	16.1094	387.70
	T	6.5085	3.5236	14.2207	6.8415	0.2927	17.6880	407.29
BS	IU	6.4807	3.4884	14.2026	6.7057	0.2960	17.3817	403.40
	F	6.4430	3.4601	14.0783	6.5974	0.2973	17.1183	400.19
	S	6.5700	3.5790	14.3745	7.0583	0.2890	18.1966	413.50
Others [1]		5.00 4.95 5.11 4.60	3.61 3.20 3.14 2.70	4.18 6.44 7.12 6.79	–	–	–	–

Table 4 Thermodynamic and elastic properties of amorphous $Ni_{36}Zr_{64}$ metallic glass

App.	SCR	$v_L/(10^3\ m\cdot s^{-1})$	$v_T/(10^3\ m\cdot s^{-1})$	$B_T/(10^9\ N\cdot m^{-2})$	$G/(10^9\ N\cdot m^{-2})$	σ	$Y/(10^9\ N\cdot m^{-2})$	θ_D/K
	H	1.8417	1.0633	1.2473	0.7484	0.2500	1.8710	132.51
	T	1.8532	1.0700	1.2631	0.7578	0.2499	1.8946	133.34
HB	IU	0.8983	0.5187	0.2968	0.1781	0.2499	0.4452	64.63
	F	0.8798	0.5080	0.2847	0.1708	0.2499	0.4270	63.30
	S	1.6398	0.9468	0.9889	0.5934	0.2499	1.4834	117.98
	H	2.7858	1.3707	3.4790	1.2438	0.3403	3.3340	172.77
	T	2.8678	1.6519	3.0356	1.8064	0.2517	4.5221	205.90
TG	IU	2.7790	1.7133	2.5216	1.9430	0.1935	4.6379	212.16
	F	2.8326	1.7600	2.5774	2.0505	0.1856	4.8621	217.77
	S	2.5452	1.4681	2.3858	1.4267	0.2507	3.5688	182.97
	H	7.3608	3.5206	24.9263	8.2046	0.3517	22.1802	444.41
	T	7.4976	3.6585	25.3982	8.8598	0.3438	23.8108	461.32
BS	IU	7.4502	3.6096	25.2429	8.6249	0.3466	23.2291	455.34
	F	7.4230	3.5900	25.0995	8.5315	0.3473	22.9898	452.91
	S	7.5667	3.7178	25.7009	9.1496	0.3409	24.5372	468.63

Table 5 Thermodynamic and elastic properties of amorphous $Ni_{50}Zr_{50}$ metallic glass

App.	SCR	$v_L/(10^3\ m\cdot s^{-1})$	$v_T/(10^3\ m\cdot s^{-1})$	$B_T/(10^9\ N\cdot m^{-2})$	$G/(10^9\ N\cdot m^{-2})$	σ	$Y/(10^9\ N\cdot m^{-2})$	θ_D/K
	H	1.7809	1.0282	1.2926	0.7755	0.2500	1.9389	132.33
	T	1.7041	0.9838	1.1835	0.7101	0.2500	1.7752	126.62
HB	IU	1.0348	0.5974	0.4364	0.2618	0.2500	0.6546	76.89
	F	1.0174	0.5874	0.4219	0.2531	0.2499	0.6328	75.60
	S	1.5031	0.8678	0.9208	0.5525	0.2500	1.3812	111.69
	H	2.6120	1.2664	3.4363	1.1766	0.3463	3.1682	164.99
	T	2.6385	1.5173	2.8551	1.6889	0.2529	4.2322	195.35
TG	IU	2.5943	1.5407	2.6153	1.7414	0.2275	4.2753	197.78
	F	2.6396	1.5804	2.6682	1.8323	0.2206	4.4730	202.72
	S	2.3400	1.3482	2.2391	1.3334	0.2516	3.3376	173.54
	H	6.8930	3.2011	24.8332	7.5170	0.3625	20.4841	417.93
	T	7.0921	3.3970	25.6101	8.4655	0.3511	22.8760	442.83
BS	IU	7.0581	3.3556	25.5318	8.2602	0.3540	22.3683	437.60
	F	7.0258	3.3297	25.3670	8.1330	0.3552	22.0433	434.29
	S	7.1585	3.4599	25.8830	8.7818	0.3476	23.6686	450.82
Others [2]		9.11 9.53	6.58 6.96	1.74 1.80	–	–	–	370.50 419.90 443.77

percentile influences of longitudinal sound velocity v_L of $Ni_{33}Y_{67}$ and $Ni_{50}Zr_{50}$ binary metallic glasses with respect to the available highest theoretical data [1,2] are found around 70.84%–85.71% and 80.46%–88.80%, respectively, while those influences of transverse sound velocity v_T are found around 76.18%–86.70% and 89.37%–93.91%. The percentile influences of isothermal bulk modulus B_T of $Ni_{33}Y_{67}$ and $Ni_{50}Zr_{50}$ binary metallic glasses with respect to the available highest theoretical data [1,2] are found around 90.45%–91.61% and 28.33%–76.63%, respectively. From Tables 2–7, it is noted that the thermodynamic and elastic properties of binary metallic glasses do not have much impact on considering screening effects. The present results computed from BS approach show higher values than those of the other two theoretical approaches. It is noted that, the inclusion of exchange and correlation effects with static H-dielectric function has enhanced the longitudinal and transverse sound velocities for HB and TG approaches, while for BS approach, suppression on both velocities is observed. No theoretical or practical data are available in the literature for any comparison of most of the binary metallic glasses, hence it is difficult to offer any remarks at this stage.

The quantitative difference between the present calculation and the experimental results, in spite of good qualitative

Table 6 Thermodynamic and elastic properties of amorphous $Ni_{60}Nb_{40}$ metallic glass

App.	SCR	$v_L/(10^3\ m\cdot s^{-1})$	$v_T/(10^3\ m\cdot s^{-1})$	$B_T/(10^9\ N\cdot m^{-2})$	$G/(10^9\ N\cdot m^{-2})$	σ	$Y/(10^9\ N\cdot m^{-2})$	θ_D/K
	H	1.8304	1.0568	1.6656	0.9994	0.2499	2.4984	147.03
	T	1.8027	1.0408	1.6156	0.9694	0.2499	2.4234	144.81
HB	IU	1.4094	0.8137	0.9874	0.5925	0.2500	1.4812	113.21
	F	1.8326	1.0581	1.6696	1.0018	0.2499	2.5044	147.21
	S	1.5655	0.9038	1.2183	0.7310	0.2500	1.8275	125.75
	H	2.6699	1.4685	3.8056	1.9298	0.2831	4.9523	205.13
	T	2.9114	1.6689	4.2619	2.4923	0.2553	6.2571	232.33
TG	IU	2.8845	1.6479	4.2055	2.4301	0.2577	6.1129	229.48
	F	2.9379	1.6798	4.3568	2.5250	0.2571	6.3485	233.90
	S	2.5714	1.4811	3.2995	1.9631	0.2518	4.9145	206.11
	H	7.3242	2.8699	38.1765	7.3701	0.4093	20.7734	407.65
	T	7.4935	3.0719	38.9887	8.4444	0.3990	23.6274	435.74
BS	IU	7.4623	3.0313	38.8671	8.2226	0.4012	23.0429	430.11
	F	7.4404	3.0118	38.7156	8.1169	0.4020	22.7602	427.38
	S	7.5481	3.1299	39.2942	8.7661	0.3962	24.4779	443.79

Table 7 Thermodynamic and elastic properties of amorphous $Ni_{81}B_{19}$ metallic glass

App.	SCR	$v_L/(10^3\ m\cdot s^{-1})$	$v_T/(10^3\ m\cdot s^{-1})$	$B_T/(10^9\ N\cdot m^{-2})$	$G/(10^9\ N\cdot m^{-2})$	σ	$Y/(10^9\ N\cdot m^{-2})$	θ_D/K
	H	1.9454	1.1232	1.6507	0.9904	0.2499	2.4760	169.68
	T	1.9799	1.1431	1.7097	1.0258	0.2499	2.5645	172.69
HB	IU	2.1866	1.2625	2.0854	1.2512	0.2499	3.1281	190.72
	F	2.1789	1.2580	2.0707	1.2424	0.2499	3.1061	190.05
	S	1.0657	0.6153	0.4954	0.2972	0.2499	0.7430	92.95
	H	2.5087	1.0074	3.8786	0.7968	0.4039	2.2371	155.27
	T	2.6200	1.2732	3.6923	1.2727	0.3454	3.4246	194.68
TG	IU	2.7686	1.2872	4.2833	1.3007	0.3621	3.5434	197.25
	F	2.7885	1.3078	4.3144	1.3426	0.3590	3.6493	200.32
	S	1.7991	1.0601	1.3649	0.8822	0.2341	2.1776	159.86
	H	6.7532	2.1969	30.7515	3.7892	0.4408	10.9190	340.28
	T	7.0940	2.6426	32.1990	5.4824	0.4194	15.5638	408.15
BS	IU	7.0602	2.5872	32.1266	5.2548	0.4224	14.9493	399.75
	F	7.0285	2.5531	31.9592	5.1175	0.4240	14.5744	394.57
	S	7.1630	2.7323	32.4663	5.8610	0.4149	16.5851	421.75

agreement, can be attributed to the following conditions: i) the sampling conditions of the experiments, ii) the short supply of data in the long wavelength region and iii) the low or high effectiveness of the local field correction functions used for the calculation of the pair potential.

From the overall picture of the present study it is noticed that, the proposed model potential is successfully applicable to study the vibrational dynamics of Ni-based metallic glasses. The influences of various local field correction functions are also observed in the present study. The experimental or theoretical data of most of the binary metallic glasses are not available in the literature, but the present study is very useful in forming a set of theoretical data of particular metallic glass.

In all the three approaches, it is very difficult to judge which approach is the best for computations of phonon dynamics of Ni-based metallic glass, because each approximation has its own identity. The HB approach is the simplest and older one, which generates consistent results of the phonon data of these glasses, because the HB approach needs minimum number of parameters. Whereas, the TG approach is developed upon the quasi-crystalline approximation in which effective force constant depends upon the correlation function for the displacement of atoms, and correlation function of displacement itself depends on the phonon frequencies. The BS approach has retained the interatomic interactions effective between the first nearest neighbors only, hence, the disorderness of the atoms in the formation of metallic glasses is more,

which shows deviation in magnitude of the PDC and their related properties. From the present study we have concluded that all the three approaches are suitable for studying the phonon dynamics of the amorphous materials. In that sense, successful application of the model potential with the three approaches is observed from the present study.

4 Conclusions

Last, it is concluded that, in the study of phonon dynamics of metallic glasses, the pair potential and its derivatives as well as pair correlation function play an important role. In the present computation, the WH form is adopted to generate the pair potentials, which ignores the angular interaction due to partially filled *d*-bands in transition metals. Most recent model potential with WH model and HB approach produces consistent results of phonon dynamics for all metallic glasses. That said, the present model potential is suitable for studying the phonon dynamics of six Ni-based metallic glasses, which confirms the applicability of the model potential in the aforementioned study. Such study on phonon dynamics of other binary as well as ternary liquid alloys and metallic glasses is in progress, which will be communicated in near future.

References

1. Pratap, A.; Bhandari, D. Saxena, N. S.; Saksena, M. P., *Ind. J. Pure & Appl. Phys.* **1994**, *32*, 128
2. Gupta, N.; Jain, K. C.; Saxena, N. S., *Phys. Status Solidi* **1993**, *176*, 81–90 (b)
3. Hubbard, J.; Beeby, J. L., *Phys. J. C: Solid State Phys.* **1969**, *2*, 556–571
4. Takeno, S.; Goda, M., *Prog. Theor. Phys*. **1971**, *45*, 331–352
5. Takeno, S.; Goda, M., *Prog. Theor. Phys*. **1972**, *47*, 790–806
6. Bhatia, A. B.; Singh, R. N., *Phys. Rev. B* **1985**, *31*, 4751–4758
7. Shukla, M. M.; Campanha, J. R., *Acta Physiol. Pol*. **1998**, *A94*, 655
8. Vora, A. M., *J. Non-Cryst. Sol*. **2006**, *352*, 3217
9. Vora, A. M., *Chin. Phys. Lett*. **2006**, *23*, 1872–1875
10. Vora A. M., *Front. Chem. China* **2011**, *6*, 54–68
11. Vora A. M., *Front. Chem. China* **2011**, *6*, 127–141
12. Vora, A. M., *J. Mater. Sci*. **2007**, *42*, 935–940
13. Vora, A. M., *Phys. A, Pol*. **2007**, *A111*, 859
14. Vora, A. M., *Front. Mater. Sci. China* **2007**, *1*, 366–378
15. Vora, A. M., *Glass Phys. Chem*. **2008**, *34*, 671–682
16. Vora, A. M., *Turkish J. Phys*. **2008**, *32*, 323
17. Vora, A. M., *FIZIKA* **2007**, *A16*, 187
18. Vora, A. M., *Romanian J. Phys*. **2008**, *533*, 517
19. Vora, A. M., *J. Struct. Chem*. **2009**, *50*, 219–227
20. Vora, A. M., *J. Non-Oxide Glass* **2009** *1*, 157
21. Vora, A. M., *Front. Mater. Sci. China* **2009**, *3*, 285–300
22. Gajjar, P. N.; Vora, A. M.; Jani, A. R., In: Proceedings of the 9th Asia Pacific Physics Conference Hanoi, Vietnam. The Gioi Publication, 2006, 429
23. Vora, A. M., In: Computational Materials, Ed. Wilhelm U. Oster, Nova Science Publishers, Inc., New York, 2009, 119
24. Harrison, W. A., Elementary Electronic Structure, World Scientific, Singapore, 1999
25. Taylor, R., *Phys. J. F: Met. Phys*. **1978**, *8*, 1699–1702
26. Ichimaru, S.; Utsumi, K., *Phys. Rev. B* **1981**, *24*, 7385–7388
27. Farid, B.; Heine, V.; Engel, G.; Robertson, I. J., *Phys. Rev. B* **1993**, *48*, 11602–11621
28. Sarkar, A.; Sen, D. S.; Haldar, S.; Roy, D., *Mod. Phys. Lett. B* **1998**, *12*, 639
29. Wills, J. M.; Harrison, W. A., *Phys. Rev. B* **1983**, *28*, 4363–4373
30. Kovalenko, N. P.; Krasny, Y. P., *Physica B* **1990**, *162*, 115–121
31. Hausleitner, C.; Hafner, J., *J. Phys.: Condens. Matter* **1990**, *2*, 6651–6657
32. Hausleitner, C.; Hafner, J., *Phys. Rev. B* **1990**, *42*, 5863–5866
33. Hausleitner, C.; Hafner, J., *Phys. Rev. B* **1993**, *47*, 5689–5709
34. Moody, D. E.; Pg, T. K., Low Temperature Specific Heat of Some Amorphous Alloys, P. Rhodes (Ed.), Physics of Transition Metals, Inst. Phys. Conf. Ser. No. 55 (Chapter 13), The Institute Of Physics, Bristol and London, 1981, 631
35. Thorpe, M. F.; *J. Non-Cryst. Sol*. **1983**, *57*, 355
36. Bretonnet, J. L.; Derouiche, A., *Phys. Rev. B* **1991**, *43*, 8924–8929